

Control Strategy for Three-Phase Grid Connected PV Inverters Enabling Current Limitation under Unbalanced Faults

Ehsan Afshari, *Student Member, IEEE*, Gholam Reza Moradi, Ramin Rahimi, Babak Farhangi, *Senior Member, IEEE*, Yongheng Yang, *Member, IEEE*, Frede Blaabjerg, *Fellow, IEEE*, and Shahrokh Farhangi, *Member, IEEE*

Abstract—Power quality and voltage control are among the most important aspects of the grid-connected power converter operation under faults. Non-sinusoidal current is injected during unbalanced voltage sag and active or/and reactive power includes double frequency content. This paper introduces a novel control strategy to mitigate the double grid frequency oscillations in the active power and dc-link voltage of the two-stage three-phase grid-connected Photovoltaic (PV) inverters during unbalanced faults. With the proposed control method, PV inverter injects sinusoidal currents under unbalanced grid faults. In addition, an efficient and easy-to-implement current limitation method is introduced, which can effectively limit the injected currents to the rated value during faults. In this case, the fault-ride-through operation is ensured and it will not trigger the overcurrent protection. A Non-MPPT operation mode is proposed for the dc-dc converter. The mode is enabled under severe faults, when the converter cannot handle the maximum PV power. Finally experimental validation is provided by implementing method in an experimental setup including a 2kW PV inverter.

Index Terms—Active power oscillations; Current limitation; dc-link voltage oscillations; Low-Voltage Ride-Through (LVRT); Photovoltaic (PV) systems.

I. INTRODUCTION

With the fast increase of grid-connected Photovoltaic (PV) generation, PV systems should contribute to the grid stability by providing ancillary services, beyond the basic power delivery [1-6]. The new grid requirements demand grid-connected PV systems, single- or three-phase, to have the capability to operate in power factors other than unity [7-9]. Also, based on the recently revised grid codes, PV inverters are preferred to stay connected during grid voltage faults [10-13]. When fault happens, the converter has to detect the incident and react quickly to the disturbance to mitigate the adverse effects

Manuscript received December 20, 2016; revised March 30, 2017 and June 14, 2017; accepted June 30, 2017. This work was supported by the Renewable Energy Organization of Iran.

E. Afshari is with the Department of Electrical and Computer Engineering, Northeastern University, Boston, MA, USA (e-mail: afshari.e@husky.neu.edu).

G. R. Moradi, R. Rahimi, and S. Farhangi are with the School of Electrical and Computer Engineering, University of Tehran, Tehran, Iran (e-mail: ghr.moradi@ut.ac.ir; raminrahimi@ut.ac.ir; farhangi@ut.ac.ir).

B. Farhangi is with the Current Ways Inc., Los Angeles, CA, USA (e-mail: farhangi@ieee.org).

Y. Yang and F. Blaabjerg are with the Department of Energy Technology, Aalborg University, Aalborg DK-9220, Denmark (e-mail: yoy@et.aau.dk; fbl@et.aau.dk).

on the inverter and the equipment connected to the grid, and also the upstream system [14-16]. Indeed, the revised grid codes require PV systems to inject a certain amount of reactive power in case of the low voltage fault, as shown in Fig. 1 [1, 4, 11, 12, 17-19]. This capability is called Low-Voltage Ride-Through (LVRT). A technical report is presented in [19], which requires the PV plants to sustain the grid fault, inject reactive power, and if possible, inject PV power to the grid. As can be seen, usually, for voltage sag depths under 0.5 p.u., the converter is not exploiting the full capacity to inject reactive power. Therefore, the remaining capacity can be utilized for generation of the active power, delivered by the PV array.

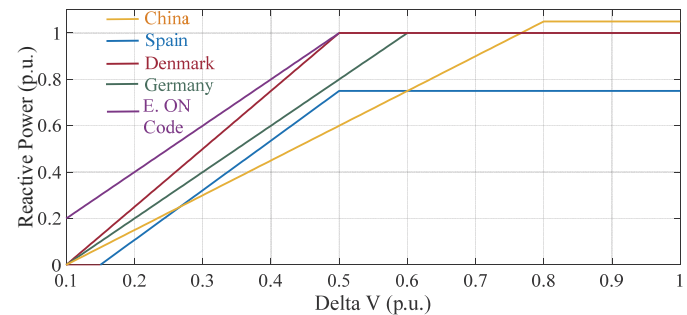


Fig. 1. The grid standard of each country, showing the reactive power should be injected to the grid during the faults, regarding the voltage sag depth.

Fundamentally, the LVRT control strategies for grid-connected PV systems under abnormal conditions should (1) quickly detect voltage faults; (2) calculate active and reactive current references in the Positive Sequence (PS) and Negative Sequence (NS); (3) prevent overcurrent failure (limit current); (4) control the dc-link voltage; and (5) control the dc-dc converter (in two-stage systems). Although the first three issues have been considered in earlier studies, the latter issues for two-stage PV systems remain untreated in details.

Once faults are detected, the current reference generation should be prioritized in the LVRT operation, as it also contributes to the current limitation. Different methods for current reference generation during grid faults have been presented in literature. In [20], the LVRT capability of the single-phase PV inverters is thoroughly discussed. In [21], a review on current reference generation of three-phase PV inverters during grid faults is performed. A few methods such as [22] have discussed the operation of a Pulse Width Modulated (PWM) grid-connected rectifier under grid faults. However, the LVRT strategy in grid-connected PV inverters is

challenging, since the dynamics of the PV panels, dc power processing stage, and the capacitive dc-link can affect the operation of the entire system. In [16, 23], an Instantaneous Active Reactive Control (IARC) was proposed, which leads to non-sinusoidal output currents under unbalanced faults. A current reference generation method dealing with both PS and NS aiming at reducing the NS of the grid voltage has been proposed in [24]. However, the active and reactive power waveforms include oscillatory components under unbalanced grid faults. In [25], the LVRT strategy controls both NS and PS to eliminate the active power oscillations under grid faults. In [26], a transformerless three-level PV inverter is introduced and the effects of the unbalanced faults on the neutral point in this inverter are analyzed for LVRT operation. The focus of [26] is on proposing new control strategies to further balance the voltage fluctuations on the neutral point under unbalanced faults. [27] has proposed a LVRT control strategy in the $d-q$ reference frame for the grid-connected converters without considering the characteristics of a renewable energy source, either PV or wind. In [28], a three-phase system has been investigated, which offers six current control freedoms with a zero-sequence current path to mitigate both active and reactive power oscillations and also inject sinusoidal currents. However, in [28], a constant dc source has been used; the negative effects of the unbalanced faults on the capacitive dc-link have not been explored. Also, in [29], the dc-link voltage is assumed to be constant. This assumption is not proper in case of an unbalanced fault as total power would not be zero and ripple would be induced to dc link voltage. Although in [30] a PV source is modeled at the input side, the performance of the proposed method is only discussed through simulations. The LVRT operation of current source grid-connected PV inverters is discussed in [31]. [32] has proposed a flexible control strategy for operation of the three-phase PV inverters under unbalanced faults; however, has not discussed control of the renewable energy source. The proposed method in [33] has improved the Dual Vector Current Control (DVCC) method to control the high peak currents and minimize the power ripple. In [34], a control strategy is proposed that balances the PS and NS components utilizing the power capacity of the inverter. However, the injected active and reactive power components still contain oscillatory harmonics. In summary on existing LVRT control challenges, in three-wire three-phase systems, in order to inject sinusoidal currents under unbalanced faults, either active or reactive power or both of them will oscillate with twice the grid fundamental frequency. To further highlight, if neither active nor reactive power oscillates, the injected currents are non-sinusoidal. The aforementioned active power oscillation can have negative impacts on reliable operation of the grid-connected PV converters. In two-stage PV converters, where a dc-dc converter operates as Maximum Power Point Tracking (MPPT), it is common that a PI controller determines the active power reference. Thus, in case that the injected active power starts fluctuating, the PI controller cannot follow the sinusoidal variations in the injected power. This is because the PV power injected to the dc-link is constant. As a result, the dc-link voltage will fluctuate with the same

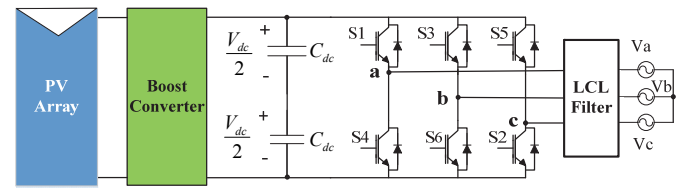


Fig. 2. Two-stage three-phase grid-connected PV system.

frequency of the injected active power. Notably, due to high failure rates of the electrolytic capacitors of the two-stage PV converters [35], the system reliability is challenged. This is worsening by dc-link voltage ripples. In this paper, dc link ripples during unbalanced faults are reduced with proper control of dc-dc converter. Among the major contributions of the paper is to investigate the effects of the PV arrays on the entire system and propose a control strategy for the PV side under unbalanced grid faults in contrast to [10, 27, 29, 33, 34, 36]; in these works, the current reference generation and grid side control have been discussed. Therefore, the operation of a two-stage grid-connected PV converter under LVRT conditions can be rarely found in the literature. Whereas, in this paper, the operation of the PV arrays, dc-dc converter, and dc-link voltage is carefully evaluated through simulations and experiments under unbalanced grid voltage sags.

In light of the above, this paper proposes (1) a new general and flexible current reference generation method that injects sinusoidal currents even under unbalanced grid faults; (2) a control method that eliminates double grid frequency oscillations from the injected active power and the dc-link voltage under unbalanced voltage sag faults, improving the long-term reliability of the PV converter; (3) a Non-MPPT operation mode for the dc-dc converter, which is enabled under severe faults, when the converter cannot handle the maximum PV power; (4) an effective current limiting method that can restrict the injected currents to the rated value. In order to realize the aforementioned advantages, the injected reactive power is allowed to oscillate with twice the grid fundamental frequency.

The paper is structured as follows: In Section II, the steady-state operation of a two-stage grid-connected PV system is presented. Section III presents the proposed LVRT strategy. Finally, the proposed algorithm is verified by simulations and also the experiments. Concluding remarks are provided at the end to summarize the advantages of the proposal.

II. SYSTEM OPERATION

This section is to analyze the inverter operation under normal and abnormal conditions for a three-wire three-phase PV system. The two-stage three-phase system is shown in Fig. 2, which includes a boost converter and a full-bridge inverter interconnected through the dc-link capacitor.

The formulation is performed in the Stationary Reference Frame (SRF). The conversion from the three-phase system into the SRF is as

$$v_{\alpha\beta} = \begin{bmatrix} v_\alpha \\ v_\beta \end{bmatrix} = \sqrt{\frac{2}{3}} \begin{bmatrix} 1 & -1/2 & -1/2 \\ 0 & \sqrt{3}/2 & -\sqrt{3}/2 \end{bmatrix} \begin{bmatrix} v_a \\ v_b \\ v_c \end{bmatrix} \quad (1)$$

where v_α, v_β are the voltages in the SRF and v_a, v_b, v_c are the

grid voltages in the natural reference frame. Since the system is three-wire, the phase currents will not contain zero sequences. Thus, the voltages and currents are obtained as:

$$v_a = V^+ \cos(\omega t + \varphi^+) + V^- \cos(\omega t + \varphi^-) \quad (2)$$

$$v_b = V^+ \cos\left(\omega t - \frac{2\pi}{3} + \varphi^+\right) + V^- \cos\left(\omega t + \frac{2\pi}{3} + \varphi^-\right) \quad (3)$$

$$v_c = V^+ \cos\left(\omega t + \frac{2\pi}{3} + \varphi^+\right) + V^- \cos\left(\omega t - \frac{2\pi}{3} + \varphi^-\right) \quad (4)$$

$$i_a = I^+ \sin(\omega t + \delta^+) + I^- \sin(\omega t + \delta^-) \quad (5)$$

$$i_b = I^+ \sin\left(\omega t - \frac{2\pi}{3} + \delta^+\right) + I^- \sin\left(\omega t + \frac{2\pi}{3} + \delta^-\right) \quad (6)$$

$$i_c = I^+ \sin\left(\omega t + \frac{2\pi}{3} + \delta^+\right) + I^- \sin\left(\omega t - \frac{2\pi}{3} + \delta^-\right) \quad (7)$$

in which, V^+ , V^- , I^+ , and I^- are the amplitudes of the positive and negative sequences of the grid voltage and current, φ^+ , φ^- , δ^+ , and δ^- are the phase angles of the grid voltage and current. The apparent power S is written as

$$S = v \cdot i^* = P + jQ \quad (8)$$

where v and i are the voltage and current vectors in the SRF, and P , Q are the active and reactive power, respectively. Since under normal conditions the grid voltages and loads are balanced, there will not be any oscillatory components in the active and reactive components of the power also the injected current is completely sinusoidal. However, under unbalanced conditions, the NS components will appear in both current and voltage vectors. Thus, the apparent power is re-written as

$$S = v_{\alpha\beta} \cdot i_{\alpha\beta}^* = (v_{\alpha\beta}^+ + v_{\alpha\beta}^-) \cdot (i_{\alpha\beta}^+ + i_{\alpha\beta}^-)^* = v_{\alpha\beta}^+ \cdot i_{\alpha\beta}^+ + v_{\alpha\beta}^+ \cdot i_{\alpha\beta}^- + v_{\alpha\beta}^- \cdot i_{\alpha\beta}^+ + v_{\alpha\beta}^- \cdot i_{\alpha\beta}^- \quad (9)$$

in which $v_{\alpha\beta}^+$ and $v_{\alpha\beta}^-$ are derived from:

$$v_{\alpha\beta}^+ = \frac{1}{2} \begin{bmatrix} 1 & -q \\ q & 1 \end{bmatrix} v_{\alpha\beta} \text{ and } v_{\alpha\beta}^- = \frac{1}{2} \begin{bmatrix} 1 & q \\ -q & 1 \end{bmatrix} v_{\alpha\beta} \quad (10)$$

where $q = e^{-j\pi/2}$ is a 90° -lagging phase-shifting operator applied to the time domain. Similarly, $i_{\alpha\beta}^+$ and $i_{\alpha\beta}^-$ are achieved following (10). In (9), there are four terms in the apparent power formulation. In (12) to (19), these terms are written as active and reactive components P_n and Q_n , where n varies from 1 to 4.

$$v_{\alpha\beta}^+ \cdot i_{\alpha\beta}^+ = (v_\alpha^+ + jv_\beta^+) \cdot (i_\alpha^+ + ji_\beta^+) = v_\alpha^+ i_\alpha^+ + v_\beta^+ i_\beta^+ + j(v_\beta^+ i_\alpha^+ - v_\alpha^+ i_\beta^+) \quad (11)$$

$$P_1 = v_\alpha^+ i_\alpha^+ + v_\beta^+ i_\beta^+ \quad (12)$$

$$Q_1 = v_\beta^+ i_\alpha^+ - v_\alpha^+ i_\beta^+ \quad (13)$$

$$P_2 = v_\alpha^+ i_\alpha^- + v_\beta^+ i_\beta^- \quad (14)$$

$$Q_2 = v_\beta^+ i_\alpha^- - v_\alpha^+ i_\beta^- \quad (15)$$

$$P_3 = v_\alpha^- i_\alpha^+ + v_\beta^- i_\beta^+ \quad (16)$$

$$Q_3 = v_\beta^- i_\alpha^+ - v_\alpha^- i_\beta^+ \quad (17)$$

$$P_4 = v_\alpha^- i_\alpha^- + v_\beta^- i_\beta^- \quad (18)$$

$$Q_4 = v_\beta^- i_\alpha^- - v_\alpha^- i_\beta^- \quad (19)$$

Multiplying two terms with the same sequences will lead to a constant term in the active and reactive power, like in (12), (13), (18), and (19). In contrast, the oscillating parts of the active and reactive power are caused by the multiplication of two terms with inverse sequences, like in (14)-(17). Therefore, the constant and oscillating parts of the total active and reactive power are written as:

$$P = P_0 + \tilde{P} \quad (20)$$

$$P_0 = P_1 + P_4 = v_\alpha^+ i_\alpha^+ + v_\beta^+ i_\beta^+ + v_\alpha^- i_\alpha^- + v_\beta^- i_\beta^- \quad (21)$$

$$\tilde{P} = P_2 + P_3 = v_\alpha^+ i_\alpha^- + v_\beta^+ i_\beta^- + v_\alpha^- i_\alpha^+ + v_\beta^- i_\beta^+ \quad (22)$$

$$Q = Q_0 + \tilde{Q} \quad (23)$$

$$Q_0 = Q_1 + Q_4 = v_\beta^+ i_\alpha^+ - v_\alpha^+ i_\beta^+ + v_\beta^- i_\alpha^- - v_\alpha^- i_\beta^- \quad (24)$$

$$\tilde{Q} = Q_2 + Q_3 = v_\beta^+ i_\alpha^- - v_\alpha^+ i_\beta^- + v_\beta^- i_\alpha^+ - v_\alpha^- i_\beta^+ \quad (25)$$

where P and Q are the total active and reactive power, P_0 , Q_0 ,

\tilde{P} , and \tilde{Q} are the constant and oscillating parts in the active and reactive power, respectively.

Under balanced voltage sag faults, there is no NS in the voltages and currents; thus, there are no oscillatory components in the active and reactive power. However, during unbalanced faults, the NS components appear in the voltages and currents. From (20) and (23), it is concluded that the active and reactive power have a constant part named P_0 and Q_0 , respectively. Also, there are two oscillating parts in the active and reactive power, denoted as \tilde{P} and \tilde{Q} . Fundamentally, in the PV power systems, all the active power generated by the PV panels are delivered to the dc-link. This active power is continuously processed by the inverter and injected into the grid. If the active power generated by the inverter is less than the power injected to the dc link from the PV source, the dc link voltage will increase; proper control is needed to synchronize the power flow from the PV source to the grid by regulating the dc link voltage. Accordingly, in the case that the injected active power has double grid frequency oscillations, the dc-link voltage will inevitably oscillate with the same frequency. Double grid frequency oscillations of the dc-link voltage have a negative impact on the life cycle of the capacitive dc-link. In the next section, a novel method to reduce such oscillations is proposed.

III. PROPOSED CONTROL SCHEME

In this section, the proposed control scheme is presented; the current reference generation method is explained and then the current limitation method is presented.

A. Current Reference Generation

In order to eliminate active power oscillations, (22) has to be zero. In (21) and (24) P_0 and Q_0 are equal to the average active power (P_{ref} which is the output of the dc-link regulator) and reactive power (Q_{ref} which is calculated during grid faults) references. These values are continuously calculated by the control algorithm as clarified in Section B. The control goal is to eliminate oscillatory components from the active power, while allowing reactive power to oscillate with the double grid frequency. Hence, \tilde{Q} is considered equal to $2(v_\beta^+ i_\alpha^- - v_\alpha^+ i_\beta^-)$, and . Accordingly, (25) is rewritten as:

$$\tilde{Q} = v_\beta^+ i_\alpha^- - v_\alpha^+ i_\beta^- + v_\beta^- i_\alpha^+ - v_\alpha^- i_\beta^+ = 2(v_\beta^+ i_\alpha^- - v_\alpha^+ i_\beta^-) \quad (26)$$

$$v_\beta^+ i_\alpha^- - v_\alpha^+ i_\beta^- - v_\beta^- i_\alpha^+ + v_\alpha^- i_\beta^+ = 0 \quad (27)$$

Furthermore, (22), (23), (25), and (28) is written as

$$\begin{bmatrix} v_\alpha^+ & v_\beta^+ & v_\alpha^- & v_\beta^- \\ v_\alpha^- & v_\beta^- & v_\alpha^+ & v_\beta^+ \\ v_\beta^+ & -v_\alpha^+ & v_\beta^- & -v_\alpha^- \\ -v_\beta^- & v_\alpha^- & v_\beta^+ & -v_\alpha^+ \end{bmatrix} \begin{bmatrix} i_\alpha^+ \\ i_\beta^+ \\ i_\alpha^- \\ i_\beta^- \end{bmatrix} = \begin{bmatrix} P_{ref} \\ 0 \\ Q_{ref} \\ 0 \end{bmatrix} \quad (28)$$

A formulation for generating sinusoidal currents to deliver a certain amount of active and reactive power is obtained as:

$$i_\alpha^+ = \frac{v_\alpha^+}{V_p - V_n} P_{ref} - \frac{v_{\alpha\perp}^+}{V_p + V_n} Q_{ref} \quad (29)$$

$$i_\alpha^- = -\frac{v_\alpha^-}{V_p - V_n} P_{ref} - \frac{v_{\alpha\perp}^-}{V_p + V_n} Q_{ref} \quad (30)$$

$$i_\beta^+ = \frac{v_\beta^+}{V_p - V_n} P_{ref} - \frac{v_{\beta\perp}^+}{V_p + V_n} Q_{ref} \quad (31)$$

$$i_\beta^- = -\frac{v_\beta^-}{V_p - V_n} P_{ref} - \frac{v_{\beta\perp}^-}{V_p + V_n} Q_{ref} \quad (32)$$

$$\begin{bmatrix} v_{\alpha\perp} \\ v_{\beta\perp} \end{bmatrix} = \begin{bmatrix} 0 & -1 \\ 1 & 0 \end{bmatrix} \begin{bmatrix} v_\alpha \\ v_\beta \end{bmatrix} \quad (33)$$

where $v_{\alpha\perp}$ and $v_{\beta\perp}$ are the orthogonal voltages (90°-lead) of the SRF voltage vectors. In the denominator of (29)-(32), there are two terms $V_p = (v_\alpha^{+2} + v_\beta^{+2})$ and $V_n = (v_\alpha^{-2} + v_\beta^{-2})$. Under balanced or even unbalanced grid faults, these terms are almost constant. Accordingly, summation or subtraction of $\sqrt{V_p}$ and $\sqrt{V_n}$ leads to a constant term, as demonstrated in Fig. 3. Therefore, the denominator in these formulations is constant and without oscillation. Notably, Q_{ref} is the average value of the reactive power required under the fault according to grid codes. Then, the SRF currents are driven from average value of the active and reactive power. These references determine the peak-peak value of the oscillations on the reactive power. The proposed formulation is customized for different objectives through definition of the following key parameters: $k_{\alpha P}$, $k_{\beta P}$, $k_{\alpha Q}$, and $k_{\beta Q}$. Accordingly, a general formulation is obtained as

$$i_{\alpha P} = \frac{v_\alpha^+ - v_\alpha^-}{(v_\alpha^{+2} + v_\beta^{+2}) + k_{\alpha P}(v_\alpha^{-2} + v_\beta^{-2})} P_{ref} \quad (34)$$

$$i_{\beta P} = \frac{v_\beta^+ - v_\beta^-}{(v_\alpha^{+2} + v_\beta^{+2}) + k_{\beta P}(v_\alpha^{-2} + v_\beta^{-2})} P_{ref} \quad (35)$$

$$i_{\alpha Q} = -\frac{v_{\alpha\perp}^+ + v_{\alpha\perp}^-}{(v_{\alpha\perp}^{+2} + v_{\beta\perp}^{+2}) + k_{\alpha Q}(v_{\alpha\perp}^{-2} + v_{\beta\perp}^{-2})} Q_{ref} \quad (36)$$

$$i_{\beta Q} = -\frac{v_{\beta\perp}^+ + v_{\beta\perp}^-}{(v_{\alpha\perp}^{+2} + v_{\beta\perp}^{+2}) + k_{\beta Q}(v_{\alpha\perp}^{-2} + v_{\beta\perp}^{-2})} Q_{ref} \quad (37)$$

in which, $i_{\alpha P}$ and $i_{\beta P}$ are the active currents in the SRF, $i_{\alpha Q}$ and $i_{\beta Q}$ are the reactive currents in the SRF, $k_{\alpha P}$, $k_{\beta P}$, $k_{\alpha Q}$, and $k_{\beta Q}$ are the key parameters, which can be either +1 or -1 to adjust the active and reactive current references in the SRF considering grid requirements. Hence, 16 modes for reference generation exist with unique features, including the active power oscillation, reactive power oscillation, and sinusoidal currents. As mentioned previously, the purpose of this paper is to present a current reference generation method to eliminate oscillations from the active power and the dc-link voltage. Simulation case studies show that only in four modes the double grid frequency oscillations can be mitigated in the injected active power, which is summarized in Table I.

TABLE I
OPERATION MODES WITH NO ACTIVE POWER OSCILLATION.

Mode	$k_{\alpha P}$	$k_{\beta P}$	$k_{\alpha Q}$	$k_{\beta Q}$
Mode 1	+1	+1	+1	+1
Mode 2	-1	-1	-1	-1
Mode 3	+1	+1	-1	-1
Mode 4	-1	-1	+1	+1

In order to exploit the full capacity of the converter, the denominator in (34)-(37) has to meet the lowest value. Thus, the key parameters are considered as listed in Mode 2 in Table I. In this case, the dc-link voltage should remain constant even if an unbalanced grid fault happens. However, it should be noted that due to the small resistances of the inductive filter, these oscillations cannot be completely eliminated from the dc-link voltage [29]. The reason is that the oscillatory components consumed by the filter's resistance, are provided by the converter.

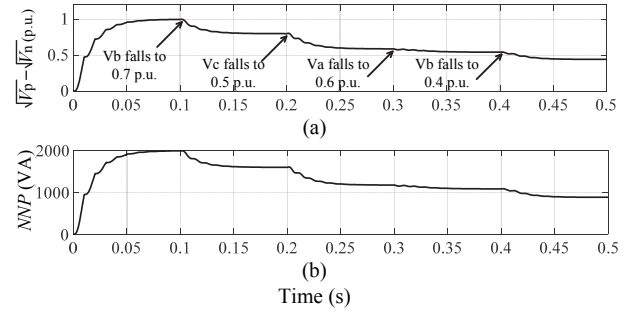


Fig. 3. Behavior of the defined parameters under the faults: (a) $\frac{\sqrt{V_p} - \sqrt{V_n}}{V_b}$ and (b) NNP – New Nominal Power.

B. Current Limitation Method

In order to prevent the overcurrent failure, a new efficient current limiting method is proposed in the following. The rated power of the converter must be updated once a voltage sag is detected; it is called New Nominal Power (NNP). Normally, under voltage sag faults, the NNP value is less than the nominal power of the converter, which depends on the voltage sag depth. Therefore, the NNP is achieved as

$$NNP = \frac{\sqrt{V_p} - \sqrt{V_n}}{V_{base}} S \quad (38)$$

where S is the apparent power or the nominal power of the power converter, V_{base} is the base voltage, which is equal to the Root-Mean-Square (RMS) value of the line-line grid voltage. In order to verify the effectiveness of this method, a simulation is performed to show that by decreasing the phase voltages, the NNP decreases, which is demanded to restrict the injected currents. At first, three-phase voltages are balanced. Then, at $t = 0.1$ s, the phase-b voltage falls to 0.7 p.u., while other phase voltages remain the same. The voltage sag orders are shown in Fig. 3. It is clearly demonstrated that the decrease in the phase voltages will result in the reduction in the NNP.

On the other hand, according to the voltage sag depth, the reactive power can be calculated as below [37].

$$\begin{cases} Q = 0 & \text{if } V_{pu} > 0.9 \\ Q = S \times 1.5 \times (0.9 - V_{pu}) & \text{if } 0.2 < V_{pu} < 0.9 \\ Q = 1.05 \times S & \text{if } V_{pu} < 0.2 \end{cases} \quad (39)$$

with V_{pu} being calculated as

$$V_{pu} = \frac{\sqrt{v_\alpha^2 + v_\beta^2}}{V_b} \quad (40)$$

Given the NNP and reactive power of Q , the maximum allowed active power (P_{max}) for the inverter to inject to the grid while avoiding overcurrent can be achieved as:

$$P_{max} = \sqrt{NNP^2 - Q^2} \quad (41)$$

For operation of the converter under very deep voltage sags, NNP will have a low value, since $\sqrt{V_p} - \sqrt{V_n}$ becomes small. Therefore, under a deep voltage sag, the condition is:

$$\text{if } (Q > NNP) \rightarrow Q = NNP, \text{ and } P_{max} = 0 \quad (42)$$

If the reactive power reference is higher than the NNP, the converter cannot inject that much reactive power to the grid. Hence, it should pick the NNP value for the reactive power reference and shed the dc power consumed from the PV arrays.

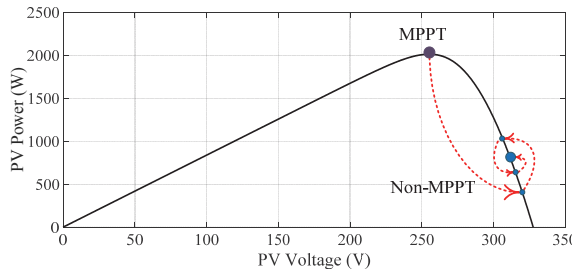


Fig. 4. P-V characteristics of the PV array. The dc-dc converter switches from MPPT to the Non-MPPT operation mode.

In summary, once a voltage sag is detected, the NNP and Q values are calculated according to (38) and (39). Then, the maximum allowed active power (P_{max}) preventing an overcurrent, is determined by (41). During the voltage sag faults, P_{max} is continuously compared with the active power reference (P^*) provided by the dc-link controller. If $P_{max} > P^*$, the exact amount of active power the converter has been injected previously can be still delivered. On the other hand, if $P_{max} < P^*$, the inverter cannot inject the active power reference (P^*) provided by the dc-link controller. In this case, in order to keep the dc-link voltage constant, the operating point of the PV arrays should move in a way to extract P_{max} from the PV array. This operation mode is called Non-MPPT mode, which would start in case a voltage sag occurs and $P_{max} < P^*$. Fig. 4 shows how the dc-dc converter is controlled in the Non-MPPT mode. The right side of the P-V characteristic is chosen for the Non-MPPT mode, since the ramp is higher; in this case, the operating point can move faster than the left side. In order to move to the right side, the duty cycle is reduced regarding (43).

$$V_{PV} = (1 - D)V_{dc} \quad (43)$$

where V_{dc} and V_{PV} are the dc-link voltage and PV voltage, respectively. Once the fault occurs and the Non-MPPT operation is activated, an approximate value for the duty cycle is calculated as

$$D_c = \frac{P_{max}}{P_{MPP}} D_{MPP} \quad (44)$$

in which D_c is the approximate value of the duty cycle for the new operating point, D_{MPP} and P_{MPP} are the duty cycle and PV power at the MPP. In Fig. 4, the left big red arrow clarifies shifting the operating point to the new position corresponded to D_c . The next smaller arrows show the operation of a PI controller adopted to tune the duty cycle of the dc-dc converter.

C. The Control Block Diagram

Fig. 5 represents the proposed control block diagram. The control structure consists of two parts, which can operate independently owing to the capacitive dc-link decoupling the two stages, dc-dc converter and inverter. A PI controller is adopted as a dc voltage regulator. The output of the PI controller determines the active power reference to stabilize the dc link voltage. The current controller block benefits from two Proportional-Resonant (PR) controllers that separately control the injected currents.

The dc-dc converter operates as the MPPT, in which the hill-climbing method is adopted. The dc-dc converter should switch to the Non-MPPT mode in case that a grid fault occurs and inverter cannot inject the maximum PV power. Fig. 6 further

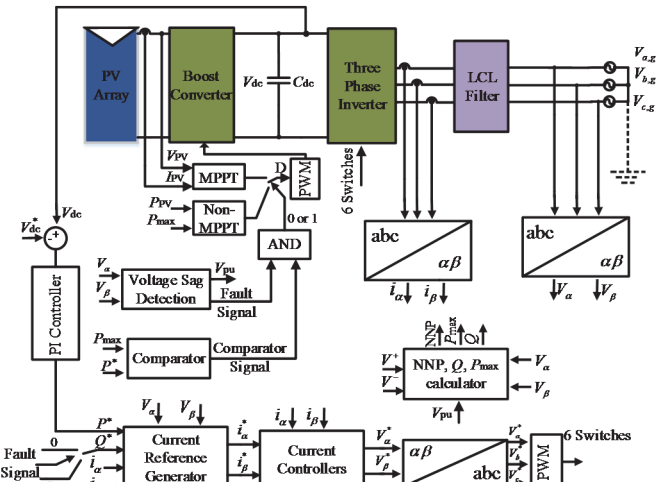


Fig. 5. Proposed control block diagram of the testbed.

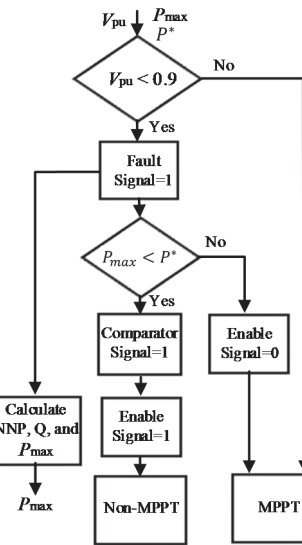


Fig. 6. Flowchart of the proposed control algorithm.

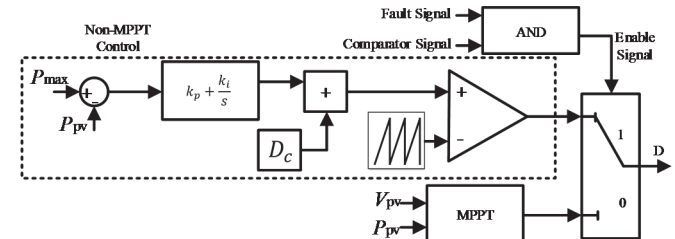


Fig. 7. Block diagram of the dc-dc converter control (MPPT vs. Non-MPPT operation).

clarifies the control system. If V_{pu} falls below 0.9 per-unit, the voltage sag detection block will generate a fault signal activating the NNP, Q, and P_{max} calculator block. Then, per a comparison between P_{max} and P^* , a comparator signal will be generated. Fig. 7 demonstrates the control of the dc-dc converter. Black dashed-line presents the Non-MPPT control algorithm, which is activated once the Enable Signal is equal to 1. D_c is the value calculated in previous section. There is an AND block, in which, if the comparator signal and fault signal are equal to 1, the dc-dc converter switches to the Non-MPPT

TABLE II
PV CONVERTER OPERATION UNDER DIFFERENT GRID CONDITIONS.

Grid Condition	LVRT	Dc-dc Converter operation
$V_{pu} > 0.9$	Disabled	MPPT
$V_{pu} < 0.9$	$\frac{P_{max} > P^*}{P_{max} < P^*}$	Enabled MPPT Enabled Non-MPPT

mode. The PI controller tunes the new duty cycle for the Non-MPPT operation. Table II summarizes the PV converter operation under different grid conditions. MPPT may continue working under abnormal operation when the fault exists in the grid and $P_{max} < P^*$. It means that the inverter has the capacity to inject maximum power of the PV array as well as the required reactive power. In this case, the fault signal is 1, while the comparator signal remains zero.

IV. SIMULATION RESULTS

A simulation testbed is developed in MATLAB/SIMULINK to verify the proposed strategy. Table III shows the power converter parameters. The dc-link voltage is assumed to be $1.3\sqrt{2}V_{L-L,rms}$, which is equal to 696 V. A case scenario is defined for verification of the proposed method, in which V_b and V_c fall to 0.45 per-unit at $t = 0.2$ s. Fig. 8(a) shows the three-phase grid voltages. Once the fault occurs, V_{pu} falls to 0.63 per-unit, LVRT operation is enabled. Fig. 8(b) shows the injected currents at the moment of the fault, which are properly controlled by the control strategy. Since the voltage sag is unbalanced, the currents in phase-b and phase-c are increased, however still restricted to 3.04 A, while phase-a decreases. However, the injected currents are purely sinusoidal. The active power is reduced; accordingly, the power extracted from the PV array is reduced by switching from the MPPT to Non-MPPT mode as shown in Fig. 8(c) and (d), respectively. Fig. 9(a) and (b) depict the injected active and reactive power, respectively, under the grid fault. Once an unbalanced voltage sag is detected, the active power is quickly reduced to 315 W (P_{max}) to prevent overcurrent failure. Although the fault is unbalanced, the active power is almost free of double frequency oscillations. Noticeably in Fig. 9(b), the injected reactive power increases to 925 VAR once the fault signal is equal to 1 and oscillates with at grid's double frequency, which is intended in the proposed method. As Fig. 9(c) illustrates, at the instant of the fault, the dc-link voltage is decreased, but after a short time, the dc-link controller reduces the active power reference, which is shown in Fig. 9(d). Fig. 9(c) shows that the dc-link voltage is properly stabilized and recovered to 696 V. Small peak-peak oscillations can be observed at the dc-link due to the double-frequency component of the power that is consumed by the filter.

TABLE III

SYSTEM PARAMETERS FOR SIMULATION AND EXPERIMENTS.

Parameters	Value
Nominal Power	2000 W
Grid line-Line voltage (RMS)	381 V, 50 Hz
Inverter side inductance of the LCL filter	6.5 mH
Grid side inductance of the LCL filter	0.65 mH
Capacitance of the LCL filter	2.2 μ F
Damping resistor of the LCL filter	5.6 Ω
Switching frequency	16 kHz
dc-link capacitor (two in series)	680 μ F

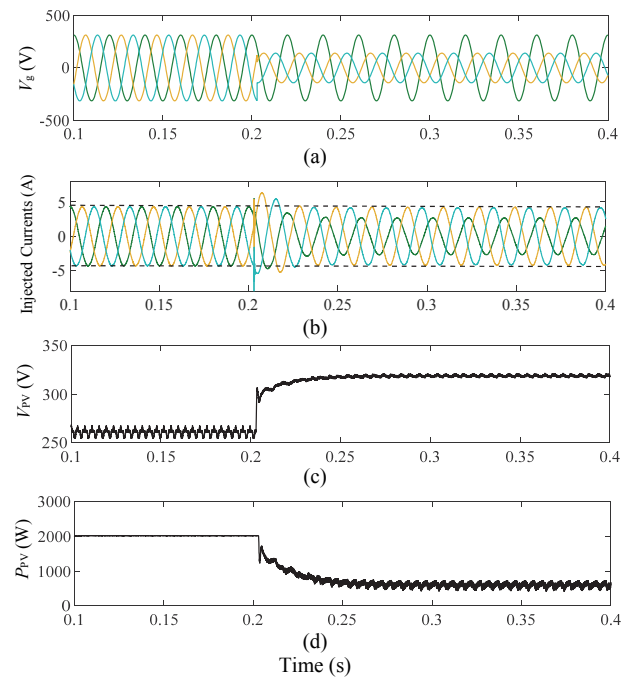


Fig. 8. Simulation results of the PV system: (a) three-phase grid voltages, (b) three-phase currents, (c) PV voltage, and (d) PV power, at the moment of the unbalanced fault.

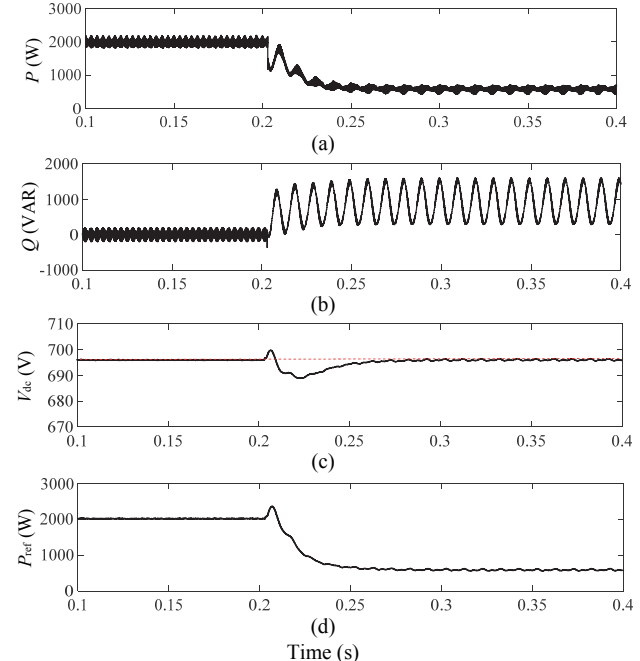


Fig. 9. Simulation results of the PV system: (a) injected active power, (b) injected reactive power, (c) dc-link voltage, and (d) output of the dc-link controller at the moment of the fault.

V. EXPERIMENTAL RESULTS

A 2-kW three-wire three-phase PV inverter is implemented to verify the proposed scheme, as shown in Fig. 10. The used PV array consists of 9 PV modules (REC 220 AE) with the maximum power of 1980 W. The parameters of the experimental setup are listed in Table III. An STM32F407VGT6 microcontroller based on ARM Cortex-M4 core is used as the digital controller. Infineon IKW40N120H3 high speed IGBTs are used for realizing both the dc-dc converter and the inverter.

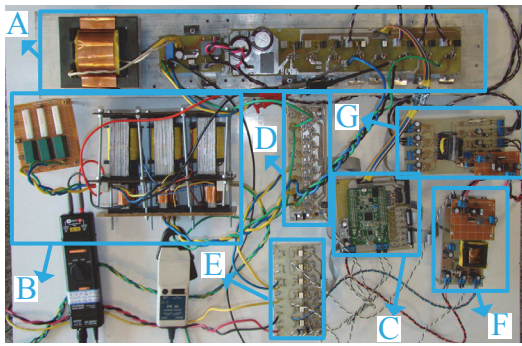


Fig. 10. Experimental setup of the implemented three-phase 2-kW PV system; A: dc-dc converter and inverter, B: LCL filter, C: control board, D: current sensor, E: voltage sensor, F and G: power supply boards.

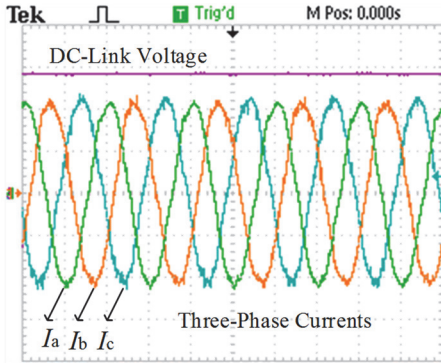


Fig. 11. Experimental results of (a) dc-link voltage (voltage [250 V/div]) and (b) injected three-phase currents under normal operation (I_a , I_b , I_c [2 A/div], time [10 ms/div]). The dc-link voltage is stabilized at 696 V.

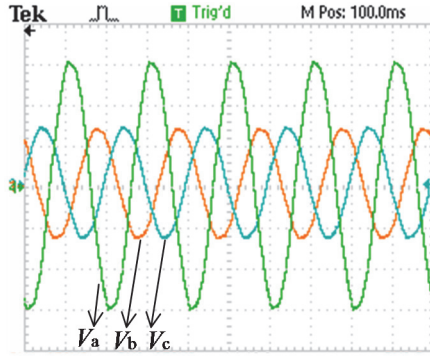


Fig. 12. Experimental results of three-phase grid voltages during the unbalanced grid fault (voltage V_a , V_b , V_c [100 V/div], time [10 ms/div]).

Fig. 11 shows the dc-link voltage and injected currents under the normal operation. At the moment of test, the irradiance was around the nominal value, so that the RMS value of the injected currents is 3 A. The dc-link voltage is stabilized at 696 V. To verify the proposed LVRT strategy, an unbalanced voltage sag is modeled by an LVRT test block. In this study, the RMS value of V_b and V_c suddenly drops to 93.5 and 94.8 V (0.425 and 0.431 p.u.), respectively, as shown in Fig. 12. Fig. 13(a) shows the dc-link voltage at the instant of the fault, which is dropped to 682 V and then recovered to 696 V within 95 ms, almost with no double frequency oscillations. Since dc power is significantly reduced at this instance (Fig. 13(b)), the currents are reduced. Then, PV power increases and results in increasing the currents. Under the experimental case study, the PV power

is reduced to prevent overcurrent failure by switching to the Non-MPPT mode. At this moment, both fault and comparator signals are equal to 1; the duty cycle changes to D_c ; afterwards, the Non-MPPT mode increases the PV voltage as shown in Fig. 13(b). Therefore, the PV current reduces, since the operating point of the P-V curve moves to the right side of the MPP. After a short time, the steady state operation point of the non-MPPT mode is reached and the phase-b current is limited to the rated value of 3.04 A.

Fig. 14(a) depicts the dc-link voltage and injected currents during the unbalanced fault. The dc-link voltage is stabilized at 696 V without any oscillations. Also, it is confirmed that the injected currents are sinusoidal even though the fault is unbalanced. Since V_b has the lowest RMS value, phase-b current is increased the most. However, the proposed strategy properly controls the phase-b current and limits it to the rated value (3.04 A), while phase-a and phase-c currents are equal to 1.75 A and 3 A, respectively. In Fig. 14(b), the PV current is decreased to 1 A, whereas the PV voltage is increased to 310 V. Thus, the PV power is decreased to 310 W to limit the injected currents. Fig. 15(a) depicts the active power during the fault. The experimental result of the active power is calculated by using the measured three-phase voltages and currents of the experimental setup, through the embedded program of the microcontroller. The data of the active power is extracted from the microcontroller and processed in MATLAB to capture the waveform. Accordingly, the active power is 310 W, being constant with low ripples. The same process is used for capturing the reactive power waveform in Fig. 15(b). It is observed that the double grid frequency oscillations exist in the reactive power, which is intended in the controller design. The average injected reactive power is 925 VAR.

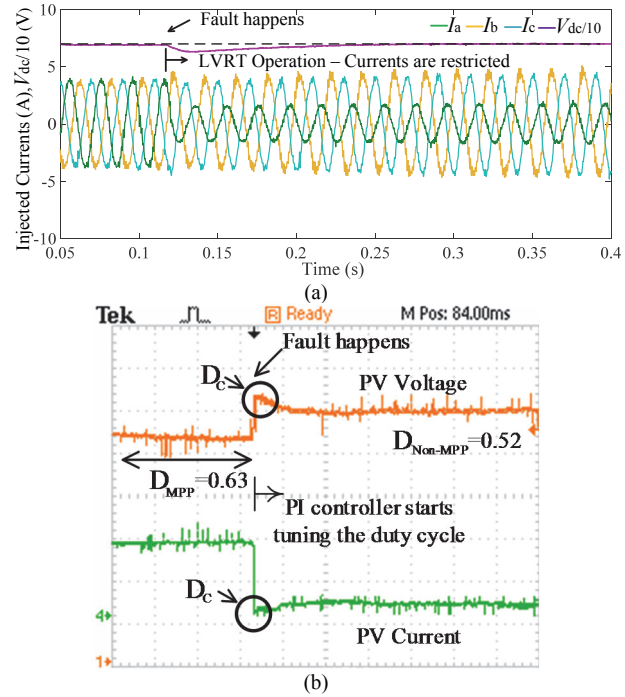


Fig. 13. Experimental results of the PV system: (a) dynamics of the injected currents and dc-link voltage (divided by 100), (b) PV voltage (voltage 50 V/div, time [50 ms/div]) and current (current 5 A/div) at the fault moment.

Table IV represents the currents THD before and during the grid fault. Since the fault is unbalanced, the THD of the three-phase currents are slightly increased; however remains lower than 5%. As reported in simulations and experiments, the active power and dc-link voltage remain almost constant, which is a major advantage over the control methods presented in [4, 14, 17, 24]. Furthermore, a very efficient current limitation method is employed, which can be easily implemented in hardware compared to the methods presented in [3, 4, 18, 24].

TABLE IV
THREE-PHASE CURRENTS THD AND RMS VALUES.

Currents	THD %	RMS (A)
Before Fault Three phase currents	4.1	3
During Fault Phase-a	4.8	1.75
During Fault Phase-b	4.3	3.04
During Fault Phase-c	4.3	3

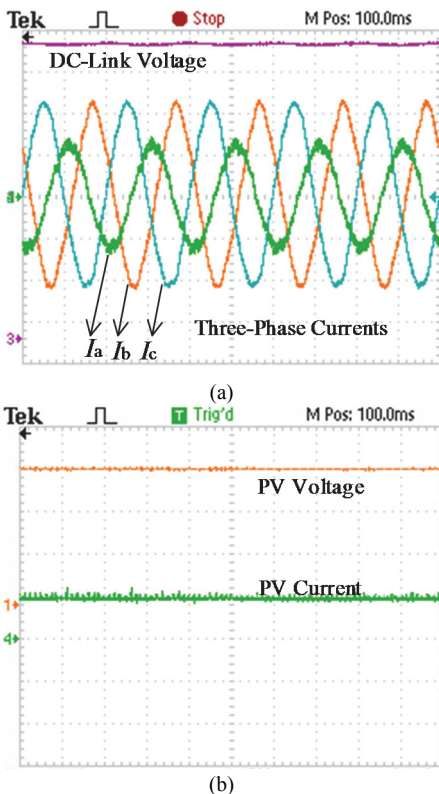


Fig. 14. Experimental results of the PV system: (a) dc-link voltage (voltage [100 V/div]) and injected three-phase currents during the unbalanced grid fault (I_a , I_b , I_c [2 A/div], time [10 ms/div]) and (b) PV current (current [1 A/div]) and PV voltage (voltage 100 V/div, time [500 us/div]), during the Non-MPPT mode during the unbalanced grid voltage sag.

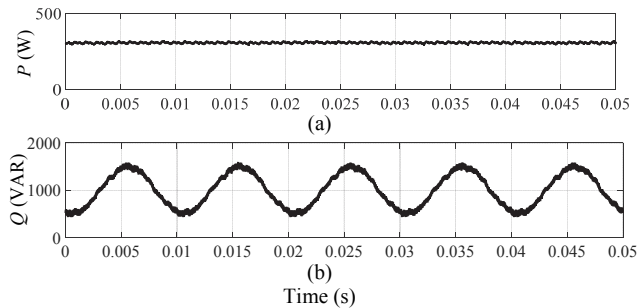


Fig. 15. Experimental results of the PV system: (a) the injected active power and (b) reactive power during the fault.

VI. CONCLUSION

This paper has proposed a novel control scheme for the three-wire three-phase two-stage PV converter to improve the power quality under abnormal conditions. Among the major contributions of the proposed method is the mitigation of the double grid frequency oscillations in the dc-link voltage and the active power under unbalanced faults. Using the proposed current reference generation, the injected currents are sinusoidal with the THD value of lower than 5% in the experiments. More importantly, the control structure benefits from two operation modes, MPPT and Non-MPPT, both of which can operate under abnormal conditions. One of the main contributions of the paper is that a Non-MPPT operation mode for the dc-dc converter is introduced and experimentally implemented. This operation mode is comprehensively investigated in this paper considering PV arrays at the input side. This feature contributes to the current limitation method that restricts the injected currents to the rated value. In contrast to the earlier current limiting methods, the proposed method benefits from a mathematical model that can be easily implemented in the embedded controller.

REFERENCES

- [1] R. Meyer, A. Zlotnik, and A. Mertens, "Fault Ride-Through Control of Medium-Voltage Converters With LCL Filter in Distributed Generation Systems," *IEEE Trans. Ind. Appl.*, vol. 50, no. 5, pp. 3448-3456, 2014.
- [2] J. Hu, Y. He, L. Xu, and B. W. Williams, "Improved control of DFIG systems during network unbalance using PI-R current regulators," *IEEE Trans. Ind. Electron.*, vol. 56, no. 2, pp. 439-451, 2009.
- [3] A. Camacho, M. Castilla, J. Miret, J. C. Vasquez, and E. Alarcon-Gallo, "Flexible Voltage Support Control for Three-Phase Distributed Generation Inverters Under Grid Fault," *IEEE Trans. Ind. Electron.*, vol. 60, no. 4, pp. 1429-1441, 2013.
- [4] J. Miret, M. Castilla, A. Camacho, L. G. d. Vicu, and J. Matas, "Control Scheme for Photovoltaic Three-Phase Inverters to Minimize Peak Currents During Unbalanced Grid-Voltage Sags," *IEEE Trans. Power Electron.*, vol. 27, no. 10, pp. 4262-4271, 2012.
- [5] R. Rahimi, E. Afshari, B. Farhangi, and S. Farhangi, "Optimal placement of additional switch in the photovoltaic single-phase grid-connected transformerless full bridge inverter for reducing common mode leakage current," in *2015 IEEE Conference on Energy Conversion (CENCON)*, 2015, pp. 408-412.
- [6] R. Rahimi, B. Farhangi, and S. Farhangi, "New topology to reduce leakage current in three-phase transformerless grid-connected photovoltaic inverters," in *2016 7th Power Electronics and Drive Systems Technologies Conference (PEDSTC)*, 2016, pp. 421-426.
- [7] E. Afshari, R. Rahimi, B. Farhangi, and S. Farhangi, "Analysis and modification of the single phase transformerless FB-DCB inverter modulation for injecting reactive power," in *2015 IEEE Conference on Energy Conversion (CENCON)*, 2015, pp. 413-418.
- [8] G. R. Moradi, E. Afshari, R. Rahimi, B. Farhangi, and S. Farhangi, "Improvement of the modulation method for single-phase transformerless photovoltaic conergy inverter for reactive power injection capability," in *2016 24th Iranian Conference on Electrical Engineering (ICEE)*, 2016, pp. 1312-1317.
- [9] C. Schauder, "Impact of FERC 661-A and IEEE 1547 on photovoltaic inverter design," in *Power and Energy Society General Meeting, 2011 IEEE*, 2011, pp. 1-6.
- [10] J. L. Sosa, M. Castilla, J. Miret, J. Matas, and Y. A. Al-Turki, "Control Strategy to Maximize the Power Capability of PV Three-Phase Inverters During Voltage Sags," *IEEE Trans. Power Electron.*, vol. 31, no. 4, pp. 3314-3323, 2016.
- [11] G. Code—High and E. H. Voltage, "Bayreuth, Germany: E," *On GmbH*, 2006.

- [12] F. Iov, A. D. Hansen, P. E. Sørensen, and N. A. Cutululis, "Mapping of grid faults and grid codes," Risø National Laboratory 8755036228, 2007.
- [13] Y. Yang, A. Sangwongwanich, H. Liu, and F. Blaabjerg, "Low voltage ride-through of two-stage grid-connected photovoltaic systems through the inherent linear power-voltage characteristic," in *Applied Power Electronics Conference and Exposition (APEC), 2017 IEEE*, 2017, pp. 3582-3588.
- [14] J. P. Mitra Mirhosseini, Vassilios G. Agelidis, "Single- and Two-Stage Inverter-Based Grid-Connected Photovoltaic Power Plants With Ride-Through Capability Under Grid Faults," *IEEE Trans. Sustain. Energy*, vol. 6, no. 3, pp. 1150-1159, 2015.
- [15] Y. Bae, T. K. Vu, and R. Y. Kim, "Implemental Control Strategy for Grid Stabilization of Grid-Connected PV System Based on German Grid Code in Symmetrical Low-to-Medium Voltage Network," *IEEE Trans. Energy Convers.*, vol. 28, no. 3, pp. 619-631, 2013.
- [16] P. Rodriguez, A. V. Timbus, R. Teodorescu, M. Liserre, and F. Blaabjerg, "Flexible Active Power Control of Distributed Power Generation Systems During Grid Faults," *IEEE Trans. Ind. Electron.*, vol. 54, no. 5, pp. 2583-2592, 2007.
- [17] G. Ding, F. Gao, H. Tian, C. Ma, M. Chen, G. He, et al., "Adaptive DC-Link Voltage Control of Two-Stage Photovoltaic Inverter During Low Voltage Ride-Through Operation," *IEEE Trans. Power Electron.*, vol. 31, no. 6, pp. 4182-4194, 2016.
- [18] W. L. Xiaoqiang Guo, Xue Zhang, Xiaofeng Sun, Zhigang Lu, and Josep M. Guerrero, "Flexible Control Strategy for Grid-Connected Inverter Under Unbalanced Grid Faults Without PLL," *IEEE Trans. Power Electron.*, vol. 30, pp. 1773-1778, 2015.
- [19] D. Energinet, "Technical regulation 3.2. 2 for PV power plants with a power output above 11 kW," *Tech. Rep.*, 2015.
- [20] Y. Yang, F. Blaabjerg, and H. Wang, "Low-Voltage Ride-Through of Single-Phase Transformerless Photovoltaic Inverters," *IEEE Trans. Ind. Appl.*, vol. 50, no. 3, pp. 1942-1952, 2014.
- [21] E. Afshari, G. R. Moradi, Y. Yang, B. Farhangi, and S. Farhangi, "A Review on Current Reference Calculation of Three-Phase Grid-Connected PV Converters under Grid Faults," in *IEEE Power and Energy Conference at Illinois (PECI)*, Illinois, USA, 2017.
- [22] P. Rioual, H. Pouliquen, and J.-P. Louis, "Regulation of a PWM rectifier in the unbalanced network state using a generalized model," *IEEE Trans. Power Electron.*, vol. 11, no. 3, pp. 495-502, 1996.
- [23] R. Teodorescu, M. Liserre, and P. Rodriguez, *Grid converters for photovoltaic and wind power systems* vol. 29: John Wiley & Sons, 2011.
- [24] C. T. Lee, C. W. Hsu, and P. T. Cheng, "A Low-Voltage Ride-Through Technique for Grid-Connected Converters of Distributed Energy Resources," *IEEE Trans. Ind. Appl.*, vol. 47, no. 4, pp. 1821-1832, 2011.
- [25] A. Junyent-Ferre, O. Gomis-Bellmunt, T. C. Green, and D. E. Soto-Sánchez, "Current Control Reference Calculation Issues for the Operation of Renewable Source Grid Interface VSCs Under Unbalanced Voltage Sags," *IEEE Trans. Power Electron.*, vol. 26, no. 12, pp. 3744-3753, 2011.
- [26] Z. Shao, X. Zhang, F. Wang, R. Cao, and H. Ni, "Analysis and Control of Neutral-Point Voltage for Transformerless Three-Level PV Inverter in LVRT Operation," *IEEE Trans. Power Electron.*, vol. 32, no. 3, pp. 2347-2359, 2017.
- [27] S. Alepuz, S. Busquets-Monge, J. Bordonau, J. A. Martínez-Velasco, C. A. Silva, J. Pontt, et al., "Control strategies based on symmetrical components for grid-connected converters under voltage dips," *IEEE Trans. Ind. Electron.*, vol. 56, no. 6, pp. 2162-2173, 2009.
- [28] K. Ma, W. Chen, M. Liserre, and F. Blaabjerg, "Power controllability of a three-phase converter with an unbalanced AC source," *IEEE Trans. Power Electron.*, vol. 30, no. 3, pp. 1591-1604, 2015.
- [29] R. Cárdenas, M. Díaz, F. Rojas, J. Clare, and P. Wheeler, "Resonant control system for low-voltage ride-through in wind energy conversion systems," *IET Power Electronics*, vol. 9, no. 6, pp. 1297-1305, 2016.
- [30] E. Afshari, B. Farhangi, Y. Yang, and S. Farhangi, "A Low-Voltage Ride-Through Control Strategy for Three-Phase Grid-Connected PV Systems" in *IEEE Power and Energy Conference at Illinois (PECI)*, Illinois, USA, 2017.
- [31] Z. Wang, B. Wu, D. Xu, M. Cheng, and L. Xu, "DC-Link Current Ripple Mitigation for Current-Source Grid-Connected Converters Under Unbalanced Grid Conditions," *IEEE Trans. Ind. Electron.*, vol. 63, no. 8, pp. 4967-4977, 2016.
- [32] X. Guo, W. Liu, and Z. Lu, "Flexible power regulation and current-limited control of grid-connected inverter under unbalanced grid voltage faults," *IEEE Trans. Ind. Electron.*, 2017.
- [33] H. C. Chen, C. T. Lee, P. T. Cheng, R. Teodorescu, and F. Blaabjerg, "A Low-Voltage Ride-Through Technique for Grid-Connected Converters With Reduced Power Transistors Stress," *IEEE Trans. Power Electron.*, vol. 31, no. 12, pp. 8562-8571, 2016.
- [34] A. Camacho, M. Castilla, J. Miret, A. Borrell, and L. G. de Vicuña, "Active and reactive power strategies with peak current limitation for distributed generation inverters during unbalanced grid faults," *IEEE Trans. Ind. Electron.*, vol. 62, no. 3, pp. 1515-1525, 2015.
- [35] H. Wang and F. Blaabjerg, "Reliability of Capacitors for DC-Link Applications in Power Electronic Converters—An Overview," *IEEE Trans. Ind. Appl.*, vol. 50, no. 5, pp. 3569-3578, 2014.
- [36] M. Castilla, J. Miret, J. L. Sosa, J. Matas, and L. G. d. Vicuña, "Grid-Fault Control Scheme for Three-Phase Photovoltaic Inverters With Adjustable Power Quality Characteristics," *IEEE Trans. Power Electron.*, vol. 25, no. 12, pp. 2930-2940, 2010.
- [37] Y. Wang, P. Yang, X. Yin, and Y. Ma, "Evaluation of low-voltage ride-through capability of a two-stage grid-connected three-level photovoltaic inverter," in *Electrical Machines and Systems (ICEMS), 2014 17th International Conference on*, 2014, pp. 822-828.



Ehsan Afshari (S'15) received B.Sc. degree in electrical engineering from Ferdowsi University of Mashhad, Mashhad, Iran, in 2013, and M.Sc. degree in electrical engineering with honors from University of Tehran, Tehran, Iran, in 2016. He is currently a PhD Candidate at the Department of Electrical and Computer Engineering, Northeastern University, Boston, MA.

His areas of interest are power electronics, design and digital control implementation of grid-connected power converters, ac-link converters, and grid integration of photovoltaic systems.



Gholam Reza Moradi received the B.Sc. degree in electrical engineering from Tafresh University, Tafresh, Iran, in 2013 and M.Sc. degree in electrical engineering from University of Tehran, Tehran, Iran, in 2016. He is currently a researcher at Department of Electrical and Computer Engineering, University of Tehran, Tehran, Iran.

His research interests include design and control of power converters for renewable energy systems, control strategies for grid integration of renewable energy sources, and digital control implementation.



Ramin Rahimi received the B.Sc. degree in electrical engineering with honors from the University of Tabriz, Tabriz, Iran, in 2013, and M.Sc. degree in electrical engineering with honors from University of Tehran, Tehran, Iran, in 2016. He is currently a researcher at the Department of Electrical and Computer Engineering, University of Tehran, Tehran, Iran.

His research interests include design, modeling, and control of power electronics converters, renewable energy systems, grid-connected transformerless photovoltaic systems, and motor drives.



Babak Farhangi (S'99-M'08-SM'15) received the B.S. and M.S. degrees from the University of Tehran, Tehran, Iran, in 2003 and 2006, respectively, and the Ph.D. degree from Texas A&M University, College Station, TX, USA, in 2014.

His research interests include power electronics and its applications in transportation electrification, renewable energy systems, micro-grids, and integrated power systems. Dr. Farhangi has been active in power electronics since 1999 through appointments in industry and academia. He has published more than 30 technical papers and one book chapter.



Yongheng Yang (S'12-M'15) received the B.Eng. degree in electrical engineering and automation from Northwestern Polytechnical University, China, in 2009 and the Ph.D. degree in electrical engineering from Aalborg University, Denmark, in 2014.

He was a postgraduate with Southeast University, China, from 2009 to 2011. In 2013, he was a Visiting Scholar at Texas A&M University, USA. Since 2014, he has been with the Department of Energy Technology, Aalborg University, where currently he is an Assistant Professor. His research includes power electronic converter design, analysis and control, and its applications in renewable energy systems.

Dr. Yang is a Member of the IEEE Power Electronics Society (PELS) Students and Young Professionals Committee. He served as a Guest Associate Editor of IEEE JOURNAL OF EMERGING AND SELECTED TOPICS IN POWER ELECTRONICS and a Guest Editor of *Applied Sciences*. He is an Associate Editor of CPSS TRANSACTIONS ON POWER ELECTRONICS AND APPLICATIONS.



Frede Blaabjerg (S'86-M'88-SM'97-F'03) received the Ph.D. degree from Aalborg University in 1995. Since 1992, he has been with Aalborg University, where he became a Full Professor in 1998. His current research interests include power electronics and its applications such as in wind and PV systems, reliability, power quality and adjustable speed drives.

He has received 18 IEEE Prize Paper Awards, the IEEE PELS Distinguished Service Award in 2009, the EPE-PEMC Council Award in 2010, the IEEE William E. Newell Power Electronics Award 2014 and the Villum Kann Rasmussen Research Award 2014. In 2017, he became Villum Investigator. He was the Editor-in-Chief of IEEE TRANSACTIONS ON POWER ELECTRONICS from 2006 to 2012. He is nominated in 2014, 2015, and 2016 by Thomson Reuters to be among the most 250 cited researchers in Engineering in the world. In 2017, he became Doctor Honoris Causa at University of Politehnica in Timisoara, Romania.



Shahrokh Farhangi (M' 90) obtained the B.Sc., M.Sc. and Ph.D. degrees in electrical engineering from University of Tehran, Iran, with honors. He is currently professor of School of Electrical and Computer Engineering, University of Tehran. His research interests include design and modeling of Power Electronic Converters, Drives, Photovoltaics and Renewable Energy Systems. He has published more than 100 papers in conference proceedings and journals. He has managed several research and industrial projects, which some of them have won national and international awards. He has been selected as the distinguished engineer in electrical engineering by Iran Academy of Sciences, in 2008.